Investigation of the Vanadyl Bond Ordering and Analysis of the Spin Exchange Interactions in $Pb_2V_3O_9$ and $Pb_2As_2VO_9$

O. Mentré*

UCCS, Equipe de Chimie du Solide, UMR CNRS 8181, ENSC Lille - UST Lille, BP 90108, 59652 Villeneuve d'Ascq Cedex, France

H.-J. Koo

Department of Chemistry and Research Institute of Basic Science, Kyung Hee University, Seoul 130-701, Korea

M.-H. Whangbo

Department of Chemistry, North Carolina State University, Raleigh, North Carolina 27695-8204

Received April 1, 2008. Revised Manuscript Received September 16, 2008

The structures of $Pb_2V_3O_9$ and $Pb_2As_2VO_9$ were determined by X-ray diffraction to settle the issue concerning whether the arrangement of the V^{4+}═O vanadyl bonds is ordered or disordered. The new crystal structure of $Pb_2V_3O_9$ refined by using a twinned crystal differs from the previous structure, determined from a combined use of powder X-ray and neutron diffraction data, and suggests an ordered Ferro arrangement of the V^{4+}═O vanadyl bonds as does the Antiferro crystal structure of the new $Pb_2As_2VO_9$. In $Pb_2V_3O_9$, a triclinic → monoclinic transition is observed at 400 °C, and the corresponding high temperature form was structurally characterized. The spin exchange interactions of $Pb_2V_3O_9$ and $Pb_2As_2VO_9$ were evaluated by performing qualitative spin dimer analysis based on tight binding calculations, and those of $Pb_2V_3O_9$ were also examined by quantitative mapping analysis based on density functional theory calculations. To a first approximation, the spin−lattice of $Pb_2V_3O_9$ is described by an alternating antiferromagnetic chain model, which is made up of the super-superexchange interactions mediated by VO_4 tetrahedra between adjacent chains of corner-sharing $V^{4+}O_6$ octahedra. The magnetic property of $Pb_2As_2VO_9$ is predicted to be paramagnetic, in agreement with experiment.

1. Introduction

The ternary magnetic oxide $Pb_2V_3O_9 = Pb_2(VO)(VO_4)_2$ is a spin gapped compound described by an alternating antiferromagnetic (AFM) chain model,[1,2] for which the ground-state is a spin singlet with an energy gap from the excited states with higher spin multiplicity. It has been found that the magnetic field above 5.2 T destroys the spin gap of $Pb_2V_3O_9$ thereby inducing a Bose-Einstein condensation (BEC) of field-induced triplets (i.e., triplons) and hence a magnetic field-induced long-range order in $Pb_2V_3O_9$.[3−7] $Pb_2V_3O_9$ is closely related to $Sr_2V_3O_9$ from the structural point of view,[8,9] but the magnetic properties of $Sr_2V_3O_9$ are described by a uniform AFM chain model.[10−12] $Sr_2V_3O_9$ adopts a monoclinic symmetry with space group $C2/c$, and the monoclinic symmetry is conserved in the $Sr_{2-x}Pb_xV_3O_9$ solid solution for x up to ∼1.5. For $\sim 1.5 < x \leq 2$, however, the solid solution adopts a triclinic symmetry with α and γ angles close to 90°.[9] At this particular transition, a gapless → spin-gap transition was observed, consistent with a possible dimerization of V^{4+} within regular chains. This monoclinic → triclinic distortion also causes a systematic twinning in the crystal samples. As a consequence, the crystal structure of $Pb_2V_3O_9$ was earlier refined by combining neutron diffraction (ND) and X-ray diffraction (XRD) data,[1] but the atomic positions, especially for vanadium, resulting from the refinement of this combined approach are contestable due to the loss of the vanadyl character for one V^{4+} position. The spin exchange interactions of $Pb_2V_3O_9$ deduced from this crystal structure are not consistent with experiment

* Corresponding author. E-mail: olivier.mentre@ensc-lille.fr.

(1) Mentré, O.; Dhaussy, A.-C.; Abraham, F.; Suard, E.; Steinfink, H. *Chem. Mater.* **1999**, *11*, 2408.
(2) (a) Waki, T.; Morimoto, Y.; Michioka, C.; Kato, M.; Kageyama, H.; Yoshimura, K.; Nakatsuji, S.; Sakai, O.; Maeno, Y.; Mitamura, H.; Goto, T. *J. Phys. Soc. Jpn.* **2004**, *73*, 3435. (b) Waki, T.; Morimoto, Y.; Kato, M.; Yoshimura, K.; Mitamura, H.; Goto, T. *Physica B* **2005**, 359–3611372.
(3) Waki, T.; Kato, M.; Morimoto, Y.; Itoh, Y.; Michioka, C.; Yoshimura, K.; Goto, T. *J. Phys. Chem. Solids* **2005**, *66*, 1432.
(4) Waki, T.; Tsujii, N.; Itoh, Y.; Michioka, C.; Yoshimura, K.; Suzuki, O.; Kitazawa, H.; Kido, G. *Physica B* **2007**, *398*, 148.
(5) Waki, T.; Michioka, C.; Itoh, Y.; Yoshimura, K. *Physica B* **2006**, 378–380148.
(6) Waki, T.; Itoh, Y.; Michioka, C.; Yoshimura, K.; Kato, M. *Phys. Rev. B* **2006**, *73*, 064419.
(7) Waki, T.; Michioka, C.; Itoh, Y.; Yoshimura, K. *J. Magn. Magn. Mater.* **2007**, *310*, 1439.
(8) Feldmann, J.; Müller-Buschbaum, Hk. *Z. Naturforsch. B* **1995**, *50*, 43.
(9) Mentré, O.; Dhaussy, A.-C.; Abraham, F.; Steinfink, H. *J. Solid State Chem.* **1998**, *140*, 417.
(10) Kaul, E. E.; Rosner, H.; Yushankhai, V.; Sischelschmidt, J.; Shpanchenko, R. V.; Geibel, C. *Phys. Rev. B* **2003**, *67*, 174417.
(11) Ivanshin, V. A.; Yushankhai, V.; Sischelschmidt, J.; Zakharov, D. V.; Kaul, E. E.; Geibel, C. *Phys. Rev. B.* **2003**, *68*, 064404.
(12) Koo, H.-J.; Whangbo, M.-H. *Solid State Sci.* **2007**, *9*, 824.

10.1021/cm800924j CCC: $40.75
Published on Web 11/05/2008

Table 1. Crystal Data and Refinement Parameters at 298 K ($C\bar{1}$ against $C1$ space group) and 823 K ($C2/c$ against Cc space group)

	$Pb_2(VO)(VO_4)_2$			
temperature	298 K		823 K	
crystal symmetry	triclinic		monoclinic	
a (Å)	7.5996(6)		7.6325(7)	
b (Å)	16.397(1)		16.500(1)	
c (Å)	6.9807(5)		6.9985(6)	
α (deg)	91.342(5)		90	
β (deg)	119.314(3)		119.501(5)	
γ (deg)	90.505(5)		90	
V (Å^3)	758.1(1)		767.1(1)	
Z	4		4	
calculated density (g/cm^3)	6.23		6.15	
μ (mm^{-1}) for Mo Kα	4.785		4.729	
equipment	Bruker X8		Bruker SMART	
radiation Mo Kα (Å)	0.71073		0.71073	
scan mode	ω/φ-scan		ω-scan	
record. ang. range 2θ (deg)	2.48−39.53		2.47−28.92	
recording reciprocal space	$-13 \le h \le 12$ $-28 \le k \le 28$ $-12 \le l \le 10$		$-9 \le h \le 10$ $-19 \le k \le 21$ $-9 \le l \le 8$	
no. measured reflns	7349/7315/23301 (1/2/composite)	1696		
T_{min}/T_{max}	0.447 (abs. in −1 Laue group)		0.458 (abs. in 2/m Laue group)	
space group	$C\bar{1}$	$C1$	$C2/c$	Cc
R int all (%)	4.18	4.18	4.60	3.61
number of independent reflections, all/[$I > 3\sigma(I)$]	7153/4536	10731/6901	578/481	1059/858
twin matrix	$hkl/\bar{h}\bar{k}\bar{l}$	$hkl/\bar{h}k\text{-}l/\bar{h}\bar{k}\bar{l}/h\bar{k}l$	none	$hkl/\bar{h}\bar{k}\bar{l}$
twin ratio (%)	56.63(6)/43.37(6)	27.83(3)/21.30(3)/28.70(3)/22.10(3)	none	46(5)/44(5)
no. ref parameters	138	63	49	63
refinement method (Jana 2000)	L.S. on F	L.S. on F	L.S. on F	L.S. on F
$R_1(F)$ [$I > 3\sigma(I)$] (%)[a]	4.25	4.49	4.92	5.01
wR_2 (F^2) [$I > 3\sigma(I)$] (%)[b]	4.65	4.99	5.54	5.76
weighting scheme	$1/\sigma^2$	$1/\sigma^2$	unit	unit
goodness of fit	1.87	1.94	0.87	0.89
isotropic sec. extinction	0.0096(7)	0.0044(7)	0.054(4)	0.052(3)
min/max $\Delta\rho$ (e/Å^3)	−2.61/2.25	−2.72/3.79	−2.62 /1.54	−2.29/1.89

[a] $R_1(F) = \sum||F_o| - |F_c||/\sum|F_o|$. [b] $wR_2(F^2) = [\sum w(F_o^2 - F_c^2)^2/\sum w(F_o^2)]^{1/2}$.

(see the spin dimer analysis of the Supporting Information).[13] In addition, among the series of related vanadyl vanadate compounds, for example, $M_2V_3O_9$ (M = Ba, Sr, Pb), it is an important issue to resolve whether the structures have an ordered or a disordered vanadyl arrangement. This latter ordering has already been contested in the case of $Sr_2V_3O_9$, while the resulting spatial distribution of Dzyaloshinski-Moriya vectors has been suggested to be responsible for the magnetic properties of this chain-like compound[10,11] In the present work, we show that the structure of a novel arsenate $Pb_2As_2VO_9 = Pb_2VO(AsO_4)_2$ has an ordered vanadyl arrangement, which is in support of an ordered vanadyl arrangement for $Pb_2V_3O_9$. It is highly desirable to determine an accurate crystal structure of $Pb_2V_3O_9$ in view of its exciting magnetic property, that is, the field-induced long-range magnetic ordering arising from BEC.

In the present work we carried out single crystal XRD refinement for $Pb_2V_3O_9$ by explicitly accounting for its twinning and by considering both Ferro ordered and disordered vanadyl chains in the crystal. The resulting crystal structure of $Pb_2V_3O_9$ differs substantially from the structure reported earlier.[1] Then, we evaluate the spin exchange interactions of $Pb_2V_3O_9$ and $Pb_2As_2VO_9$ by spin dimer analysis based on tight binding calculations.[14] The spin exchange interactions of $Pb_2V_3O_9$ were also examined by performing quantitative mapping analysis based on first principles density functional theory (DFT) calculations.[14a]

(13) The spin dimer analysis using the crystal structure of $Pb_2V_3O_9$ reported in ref 1 leads to the conclusion that $Pb_2V_3O_9$ has two different kinds of antiferromagnetic alternating chains, which is inconsistent with experiment.

2. Experimental Section

Twinned crystals of PbV_2O_6 used in our study were grown by electrosynthesis as described in refs 1 and 9. We used a X8 Bruker single crystal diffractometer for data collection at room temperature, and a Bruker SMART diffractometer for data collection at high temperature (550 °C) with the crystal enclosed in a quartz capillary. The heating device consisted of a goniometer head assorted with a hot air blower. The temperature was controlled by a thermocouple located at ∼5 mm from the crystal.

The powder sample of $Pb_2As_2VO_9$ was prepared by solid state reaction (600 °C) between $Pb_2As_2O_7$ and VO_2 in evacuated tubes for 4 days. $Pb_2As_2O_7$ was previously prepared at 600 °C from PbO, and As_2O_5 mixture. Single crystals have been obtained from the melting at 850 °C of a mixture of PbO, As_2O_5, and VO_2 in the 2:1:1 ratio. Crystal data were collected on Bruker SMART diffractometer. The magnetic susceptibility of $Pb_2As_2VO_9$ was measured on a Oxford Maglab EXA 9T extraction magnetometer on cooling under an applied field of 1 T.

3. Crystal Structure Determination

The crystal data and refinement parameters of $Pb_2V_3O_9$ and $Pb_2As_2VO_9$ are summarized in Tables 1 and 2, respectively. In what follows, we describe our structure determination in detail.

3.1. Processing of the Twinned Data for $Pb_2V_3O_9$. The inaccuracy of the previously reported $Pb_2V_3O_9$ crystal structure[1] stems from its refinement using both XRD and

Table 2. Crystal Data and Refinement Parameters at 298 K for $Pb_2As_2VO_9$

temperature	298 K
crystal symmetry	monoclinic
a (Å)	7.565(2)
b (Å)	16.473(4)
c (Å)	6.956(2)
β (deg)	120.07(1)
V (Å^3)	750.1(3)
Z	4
calculated density (g/cm^3)	6.72
μ (mm^{-1}) for Mo Kα	5.78
equipment	Bruker SMART 1K
radiation Mo Kα (Å)	0.71073
scan mode	ω-scan
record. ang. range 2θ (deg)	2.47−31.65
recording reciprocal space	$-10 \le h \le 10$ $-23 \le k \le 23$ $-10 \le l \le 9$
no. measured reflns	4517
T_{min}/T_{max}	0.32
space group	$P2_1/n$
R int all (%)	5.32
number of independent reflections, all/[$I > 3\sigma(I)$]	1368/1154
twin matrix	no twin
no. ref parameters	83
refinement method (Jana 2000)	L.S. on F
$R_1(F)$ [$I > 3\sigma(I)$] (%)[a]	4.42
wR_2 (F^2) [$I > 3\sigma(I)$] (%)[b]	4.43
weighting scheme	unit
goodness of fit	2.98
isotropic sec. extinction	0.015(1)
min/max $\Delta\rho$ (e/Å^3)	−1.78/2.55

[a] $R_1(F) = \sum||F_o| - |F_c||/\sum|F_o|$. [b] wR_2 $(F^2) = [\sum w(F_o^2 - F_c^2)^2/\sum w(F_o^2)]^{1/2}$.

ND data. In fact, the sample of $Pb_2V_3O_9$ is textured such that strong preferred orientations are evident in the XRD data. Furthermore, vanadium is almost transparent to neutron elastic scattering, and this introduces a certain degree of inaccuracy in the assignment of the V positions.[1] A strong clue to the incorrectness of the published structure was the loss of the vanadyl (i.e., V═O) character for one of the V^{4+} cation positions, unlike the case of the analogous compound $Sr_2V_3O_9$ in which chains of corner-sharing VO_6 octahedra exhibit alternating long O···V and short V═O distances.[8,9] In the previously reported crystal structure for $Pb_2V_3O_9$, the V(3)b position is correct while V(3)a forms a short V—O bond of 1.72 A, which is too long for a standard vanadyl V^{4+}═O bond. Furthermore, this bond is created toward an oxygen atom already strongly engaged in a short tetrahedral V^{5+}—O bond. The bond valence sum calculated for this oxygen atom leads to an abnormally high value of −2.53 for oxygen, which is characteristic of an overbonded character.

The crystal structure of $Pb_2V_3O_9$ was refined using the XRD data of a twinned crystal. The pseudomerohedral twinning of the crystal samples is systematic and inherent to domains created by the triclinic/pseudomonoclinic distortion occurring in this compound. The twinning law has already been described in ref 1 and emulates the 2/m Laue group of the more symmetric monoclinic related compounds $Sr_{2-x}Pb_xV_3O_9$. The C-centered triclinic unit cell was arbitrarily chosen by analogy with $Sr_2V_3O_9$. The twin law

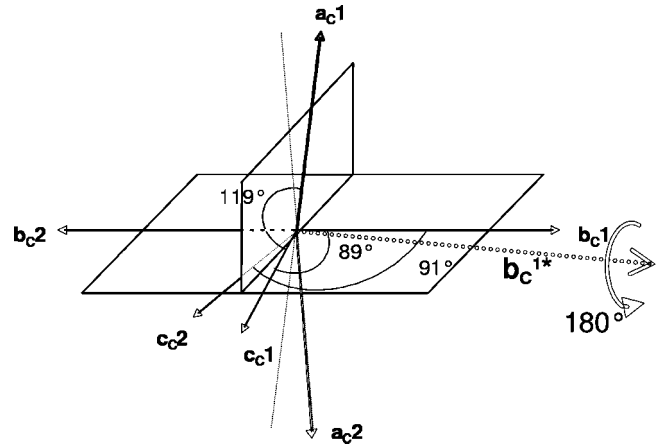

Figure 1. Scheme of the imbrication of the two lattices by twinning in $Pb_2V_3O_9$.

requires a rotation of 180° about the b_c* axis, which yields the splitting of a_c* and c_c* into a_c*1, c_c*1 and a_c*2, c_c*2 while b_c* remain unique. The imbrications of the two crystal lattices are schematically shown in Figure 1, which are consistent with the splitting of all reflections except for those in the $h0l$ layer. The basal R* layers reconstructed from the collected frames are presented in Figure S1 of the Supporting Information. It confirms the good quality of the crystals apart from the twinning. The subsequent XRD data processing and crystal structure refinement were divided in the following stages:

(i) The lattice parameters, the orientation matrices for each domain and the twin law are found from a "peak hunting" file containing a significant number of diffracted intensities ($n > 1000$) using the program CELL-NOW.[15] The reflections are fully indexed by taking into consideration two main partially overlaping domains. The results are consistent with the twin previously reported (180° about b*).

(ii) After the data collection was optimized from the main domain matrix (domain 1) to cover the full reciprocal lattice, the intensities were integrated from the frames using SAINT 7,[16] and the two orientation matrices. It leads to three series of data, that is, the domain 1, the domain 2, and the overlapping reflections.

(iii) Absorption corrections were performed using the program TWINABS[15] from equivalent and redundant reflections. The data were fit to a single dominant component by modeling the absorption surfaces. The data were corrected using equivalent reflections and Friedel pairs, regardless of whether or not the selected space group is centrosymmetric, due to the nearly centrosymmetric positions for all the atoms except for the V^{4+}cations as explained later. However, the data were subsequently merged into the two possible point groups, namely, 1 and −1.

(iv) The crystal structure was refined starting from the published model (ref 1) using Jana 2000[17] by considering

(14) For reviews see: (a) Whangbo, M.-H.; Koo, H.-J.; Dai, D. *J. Solid State Chem.* **2003**, *176*, 417. (b) Whangbo, M.-H.; Dai, D.; Koo, H.-J. *Solid State Sci.* **2005**, *7*, 827.

(15) Sheldrick, G. M. *Cell_Now- Twinabs*; University of Göttingen: Göttingen, Germany, 2003.

(16) Bruker. *SAINT-Plus*, Version 6.35A; Bruker AXS Inc.: Madison, WI, 2002.

(17) Petricek, V.; Dusek, M.; Palatinus, L. *Jana 2000*; Institute of Physics: Praha, Czech Repubic, 1997.

both isolated and composite intensities for the components 1 and 2, which leads to the twin ratio using the relation for intensities:

$$F^2=(\mathrm{OSF})^2\sum_{m=1}^{n} k_m {F_m}^2$$

where the OSF refers to the overall scale factor, k_m is the fractional contribution of the twin domain m, and n is the number of domains.

3.2. Room-Temperature Structure of $Pb_2V_3O_9$: Ferro-Ordering versus Random Distribution. In most cases, an ambiguity about the V^{4+} positions remains even after crystal structure refinement. It stems from the location of pseudo-inversion centers at the centers of the $V^{4+}O_6$ octahedra, leading to the split of the V^{4+} cation position off the special position toward one corner of its surrounding O_6 octahedron. It creates one long O···V and one short V═O bond. For instance, $Sr_2V_3O_9$ and several $Sr_{2-x}Pb_xV_3O_9$ compounds are described in terms of half-occupied V^{4+} sites to avoid two V^{4+} cations per octahedron, which leads to disordered vanadyl bonds within chains of corner-sharing octahedra.[8,9] From the crystallographic point of view, a uncertainty exists due to the fact that the ordered model ($C1$ space group) and the disordered model ($C\bar{1}$ space group) give rise to nearly similar XRD intensities. The ordered model generally leads to racemic twinning, while the disordered model (i.e., only one V^{4+} cation per $Pb_2V_3O_9$ formula unit) breaks the centric character. In such cases, the crystallographic standard principles favor the most symmetrical symmetry, but the unambiguously fully ordered arrangement of the V^{4+}═O bonds in $Pb_2As_2VO_9$ (see below) validates the notion of ordered vanadyl bonds. Similarly, an accurate analysis of $Pb_2V_3O_9$ from several crystallochemical characteristics enables one to suggest the true "hidden" space group according to a Ferro vanadyl arrangement in the crystal.

In isolated chains of corner-sharing distorted VO_6 octahedra, the "overbonded" character of oxygen with two short vanadyl bonds (i.e., V═O═V) should be avoided by introducing a cooperative displacement (Figure 2a). For similar reasons the $P2_1$ space group was favored over $P2_1/m$ for $Ba_2V_3O_9$ containing rutile-like vanadyl chains.[18,19] In the *ac*-plane the interchain cooperative displacement of the V^{4+} cations within the V_3O_9 layers should be imposed by the lattice translation. Otherwise, the unit cell would be quadrupled (i.e., $2a \times 2c$), but this was not observed by XRD data (Figure 2b). The correlation between vanadyl-chains in the same layer remains an open question in $Sr_2V_3O_9$, and the energy difference between the ferro and the antiferro V^{4+}═O arrangements is expected to be small.[10,11] Indeed, full "on-site" V^{4+} disorder would also yield an apparently C-centered-like diffraction pattern. However, it is clear that the cooperative displacements of the V^{4+} ions in single chains should weaken the amplitude of the disorder. Furthermore, the analysis of the in-plane $V^{4+}-V^{5+}$ distances in the disordered model show a distribution of short (3.41 and 3.44 Å) and long (3.54 and 3.56 Å) V···V distances. Only the 2D-ferro ordering of V^{4+}═O leads to a regular V^{4+}/V^{5+} arrangement with alternating short and long V···V distances. The disorder in each layer would create crystallographically equivalent V^{4+}═O chains surrounded on both sides by V^{5+} ions with only short V···V distances (~3.43 Å) and other chains surrounded on both sides only by V^{5+} ions with long V···V distances (~3.55 Å). Such an arrangement arising from the disorder should be highly unstable. In addition, the disorder should bring local defects, which we did not observe in the crystal diffraction patterns, Figure S1, Supporting Information.

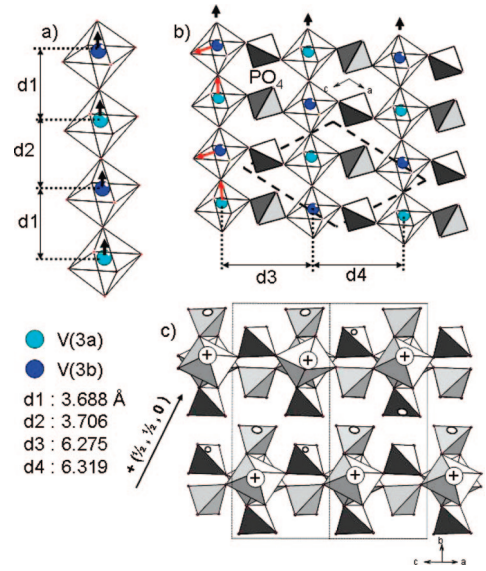

Figure 2. $Pb_2V_3O_9$ crystal structure at 298 K. (a) Corner sharing vanadyl chains. (b) Cooperative V═O bonds in layers parallel to the (*a*,*c*) plane. The red arrows describe the previously reported V═O arrangement from ref 1. (c) Cooperative vanadyl bonds between layers due to the C-centering.

The random interlayer organization of the V═O displacement is unlikely and should be excluded while retaining the C-centered Bravais lattice. The driving force for this ordering is more likely the regular alternation of $V^{4+}-V^{5+}$ distances and $V^{4+}-Pb^{2+}$ distances rather than a random arrangement of these distances. In addition, from the magnetic point of view it is worth recalling that the random combination of several $V^{4+}-O-O-V^{4+}$ SSE paths would likely kill the gap, as observed in the $BiCu_2(P_{1-x}V_x)O_6$ system. Here, a magnetically gapped system transforms to the gapless system for x values in which incommensurate ordering "almost randomly" combinates a number of $Cu^{2+}\cdots Cu^{2+}$ interactions.[20] Then, the $1/2(\vec{a}+\vec{b})$ translation gives rise to the ordered displacement for the V^{4+} cations yielding the possible true space group $C1$ (Figure 2c). Taking into account the twinning described above, the refinement was first performed in the centrosymmetric $C\bar{1}$ leading to accurate positions for all atoms but disordered vanadyl bonds with R = 4.25% and wR = 4.65%. During the refinement in the true $C1$ space group, the oxygen atoms were fixed to their ideal positions deduced from the $C\bar{1}$ model due to strong correlations between the atoms related by a center of

(18) Feldmann, J.; Müller-Buschbaum, Hk. *Z. Naturforsch.* **1996**, *51*, 489.
(19) Dhaussy, A.-C.; Abraham, F.; Mentré, O.; Steinfink, H. *J. Solid State Chem.* **1996**, *126*, 328.
(20) Mentré, O.; Ketatni, E. M.; Colmont, M.; Huvé, M.; Abraham, F.; Petricek, V. *J. Am. Chem. Soc.* **2006**, *128*, 10857.

Table 3. Atomic Coordinates and Isotropic/Equivalent Thermal Parameter at Room Temperature (*C*1 space group)[a]

atom	*x*	*y*	*z*	U_{iso}
Pb1a[i]	−0.0019(6)	−0.1230(3)	0.2251(8)	0.0207(5)
Pb1b	0.0011(6)	0.1239(3)	−0.2234(8)	0.0169(4)
Pb2a	0.0106(6)	0.4544(3)	0.2513(8)	0.0249(5)
Pb2b	−0.0105(6)	−0.4522(3)	−0.2460(8)	0.0213(5)
V1a[ii]	0.0136(8)	0.6622(4)	0.2623(9)	0.0084(4)
V1b	−0.0093(8)	−0.6587(4)	−0.2547(9)	0.0085(5)
V2a	−0.0055(8)	0.0805(4)	0.2593(9)	0.0098(8)
V2b	0.0064(8)	−0.0807(4)	−0.2568(9)	0.0074(8)
V3a	0.2804(7)	0.2447(4)	0.5337(8)	0.0102(5)
V3b	0.7813(7)	0.2558(4)	0.0313(8)	0.0127(5)
O1a[iii]	−0.5033(7)	0.2141(3)	0.2251(8)	0.0207(5)
O1b	0.5033(7)	−0.2141(3)	−0.2234(8)	0.0169(4)
O2a	0.1243(7)	0.1441(3)	0.2513(8)	0.0249(5)
O2b	−0.1243(7)	−0.1441(3)	−0.2460(8)	0.0213(5)
O3a	−0.1610(6)	0.1363(3)	−0.2525(7)	0.0118(2)
O3b	0.1610(6)	−0.1363(3)	0.2525(7)	0.0118(2)
O4a	0.1516(6)	0.7329(3)	0.4949(7)	0.0147(2)
O4b	−0.1516(6)	−0.7329(3)	−0.4949(7)	0.0147(2)
O5a	−0.1792(7)	0.7108(3)	0.0188(7)	0.012(2)
O5b	0.1792(7)	−0.7108(3)	−0.0188(7)	0.012(2)
O6a	−0.1582(7)	0.0148(3)	0.2115(7)	0.014(2)
O6b	0.1582(7)	−0.0148(3)	−0.2115(7)	0.014(2)
O7a	0.1575(7)	0.0239(3)	0.2757(7)	0.016(2)
O7b	−0.1575(7)	−0.0239(3)	−0.2757(7)	0.016(2)
O8a	−0.0831(7)	0.5896(3)	0.2904(7)	0.016(2)
O8b	0.0831(7)	−0.5896(3)	−0.2904(7)	0.016(2
O9a	0.1481(7)	0.6087(3)	0.2217(7)	0.019(2)
O9b	−0.1481(7)	−0.6087(3)	−0.2217(7)	0.019(2)

[a] The Pb atoms were treated anisotropically but the vanadium atoms isotropically. The oxygen coordinates and their anisotropic thermal parameters were fixed according to their refined values in the centrosymmetric model.

symmetry. In addition, due to the loss of the symmetry center, two additional racemic twins were added and refined. The final R = 4.48% and wR = 5% are in good support of the proposed model (Table 1). The final atomic coordinates are listed in the Table 3. Furthermore, the weak residual density located at the removed V^{4+} position is in agreement with the cooperative displacement of the vanadyl groups in the whole crystal. Of course, from the refinements in *C*1 and $C\bar{1}$ space groups, an ambiguity remains between the Ferro ordering and disordered model without the direct probing of the absence of inversion center. It is worth recalling that the disordered model should simultaneously lead to (a) fully disordered domains (apparent C lattice with a large number of local defects for reasons explained above) and (b) partially disordered domains, as well as (c) smaller mostly ferro (apparent C lattice) and (d) mostly antiferro domains (apparent P lattice). Here, diffuse scattering phenomena should be observed in the full reciprocal lattice, at least on the C-forbidden *hkl*, $h + k = 2n + 1$ lines not observed on the reconstructed diffraction patterns, Supporting Information. The selected interatomic distances of $Pb_2V_3O_9$ at 298 K in the *C*1 space group are listed in Table 4.

The refined structure shows the alternation of $V^{4+}-V^{4+}$ distances along the corner-sharing vanadyl chains (i.e., d1 = 3.688(6) Å and d2 = 3.706(6)Å) and also along the corner-sharing octahedral/tetrahedral chains (i.e., d3 = 6.275(9) Å and d4 = 6.319(9) Å) (Figure 2a). Finally, the final calculated bond valence sum for octahedral/tetrahedral common oxygen corner is calculated to be −1.92, much more plausible that the value of −2.53 previously calculated. Thus, the previously published model should definitively be discarded.

3.3. Effect of Temperature on the Structure of $Pb_2V_3O_9$. Figure 3 shows the XRD patterns of powdered $Pb_2V_3O_9$ samples as a function of temperature under flowing nitrogen. Around 400 °C the coalescence of the *hkl*/$h^{-}kl$ pairs is observed, which suggests a triclinic → monoclinic transition. This transition was confirmed by single crystal thermodiffraction measurements using the apparatus described in the experimental section. In fact, the transition is easily observed because the splitting of spots disappears due to the twinning (triclinic symmetry) toward a unique spot in the monoclinic domain. After determining the lattice parameters every 50 °C on heating, the transition was observed at 500 °C. The data collection was performed at 550 °C. The discrepancy between the temperature transition deduced from the powder and single crystal experiments is most probably caused by the distance between the thermocouple and the sample in the latter experiment while the thermalization of the sample was optimal in the former experiment. The alternating $V^{4+}{=}O\cdots V^{4+}{=}O$ schemes of the RT and HT forms are compatible, hence providing additional evidence for the validity of the here refined RT model. The transition from the HT to the LT form is displacive and reversible; no DTA signal was detected under flowing nitrogen.

For reasons similar to those presented in the previous RT analysis, the crystal structure of $Pb_2V_3O_9$ at 550 °C was refined both in the *C*2/*c* and *Cc* space groups. The acentric space group *Cc* was found to be better (Table 1), and leads to a fully ordered model with no significant residual electron density peaks remaining on the removed V^{4+} cation centers. The atomic coordinates are shown in Table 5. The crystal structure evolution as a function of temperature is mainly driven by the expansion of the *b*-axis length, which is related to the interlayer interaction. The VO_6/VO_4 assembly remains nearly unchanged while most significant changes occur around the Pb coordination sphere. The pertinent interatomic distances are listed in Table 4. Within the layers the monoclinic structure leads to only one $V^{4+}-V^{4+}$ distance along the edge-sharing vanadyl chains (i.e., 3.700(9) Å) and also along the direction perpendicular to them (i.e., 6.32(2) Å). The anisotropic thermal parameters for the Pb atoms at room temperature and at 550 °C are listed in Table S1 of the Supporting Information.

3.4. Antiferro Displacements of the $V^{4+}{=}O$ Bonds between the As_2VO_9 Layers in $Pb_2As_2VO_9$. The details of the crystal structure refinement for $Pb_2As_2VO_9$ by using Jana 2000[17] are summarized in the Table 6. The anisotropic thermal parameters are given in Table S2, Supporting Information. In contrast to the case of $Pb_2V_3O_9$, $Pb_2As_2VO_9$ crystallizes in the space group $P2_1/n$. Due to the primitive-monoclinic Bravais lattice, the inversion centers lie in between two As_2VO_9 layers (Figure 4a) so that there is no ambiguity about the V^{4+} ions lying on a single fully occupied 2(a) position. Then, the $V^{4+}{=}O$ arrangement remains cooperative within the As_2VO_9 layers parallel to the ac-plane while it is reversed between them. The interslab vanadyl bond arrangements in $Pb_2V_3O_9$ (ferro) and $Pb_2As_2VO_9$ (anti-ferro) are compared in Figure 4.

The unit cell volume is nearly unchanged in $Pb_2V_3O_9$ and $Pb_2As_2VO_9$ (i.e., ∼758 and ∼750 $Å^3$, respectively), and there

Table 4. Selected Interatomic Distances of $Pb_2V_3O_9$ at $T = 298$ and 823 K

$T = 298$ K (S.G. *C*1)	Pb^{2+} polyhedra	V^{5+} tetrahedra	V^{4+} octahedra				
Pb1a−O2b	2.572(6)	Pb2a−O1b	2.765(5)	V1a−O4a	1.713(7)	V3a−O1a	1.682(4)
−O3b	2.556(6)	−O2b	2.975(5)	−O5a	1.716(7)	−O1b	2.187(4)
−O4a	2.665(5)	−O3b	2.778(4)	−O8a	1.750(6)	−O2a	1.957(6)
−O6a	2.697(6)	−O6a	2.582(5)	−O9a	1.692(6)	−O2b	2.008(6)
−O7a	2.695(5)	−O7a	2.841(5)			−O5a	2.036(7)
−O8b	2.839(4)	−O8a	2.583(5)	V1b−O4b	1.748(7)	−O5b	1.965(7)
−O9b	2.439(4)	−O8b	2.484(6)	−O5b	1.740(7)		
		−O9a	2.892(5)	−O8b	1.679(6)		
		−O9b	2.814(6)	−O9b	1.703(6)		
Pb1b−O2a	2.586(6)	Pb2b−O1a	2.731(5)	V2a−O2a	1.755(6)	V3b−O1a	2.188(4)
−O3a	2.539(6)	−O2a	2.961(4)	−O3a	1.790(6)	−O1b	1.696(4)
−O4b	2.647(5)	−O3a	2.753(4)	−O6a	1.670(7)	−O3a	2.022(6)
−O6b	2.716(6)	−O6b	2.582(5)	−O7a	1.671(7)	−O3b	1.959(6)
−O7b	2.702(5)	−O7b	2.869(5)			−O4a	1.981(7)
−O8a	2.846(4)	−O8a	2.440(6)	V2b−O2b	1.765(6)	−O4b	2.007(7)
−O9a	2.439(4)	−O8b	2.599(5)	−O3b	1.776(6)		
		−O9a	2.832(6)	−O6b	1.675(7)		
		−O9b	2.937(5)	−O7b	1.670(7)		

$T = 823$ K (S.G. *Cc*)		Pb^{2+} polyhedra		V^{5+} tetrahedra		V^{4+} octahedra	
Pb1−O2a	2.6(6)	Pb2−O1	2.79(2)	V1−O4a	1.71(4)	V3−O1	2.25(4)
−O2b	2.83(6)	−O2a	2.78(6)	−O4b	1.72(4)	−O1	1.62(4)
−O3a	2.46(4)	−O2b	2.74(6)	−O5a	1.72(5)	−O3a	1.99(3)
−O3b	2.68(4)	−O3b	2.76(3)	−O5b	1.69(5)	−O3b	1.97(3)
−O4a	2.70(4)	−O4a	2.73(4)			−O5a	2.07(5)
−O4b	2.56(4)	−O4a	2.55(5)	V2−O2a	1.64(6)	−O5b	1.98(5)
−O5a	2.78(4)	−O4b	2.75(6)	−O2b	1.65(6)		
−O5b	2.97(4)	−O4b	2.81(4)	−O3a	1.80(3)		
				−O3b	1.73(3)		

is no significant change in the X−O bond lengths of the XO_4 tetrahedra (close to 1.7 Å). The selected interatomic distances of $Pb_2As_2VO_9$ at 298 K are listed in Table 7. In understanding the difference between the V^{4+}═O arrangements of the two compounds, it is important to note that $Pb_2As_2VO_9$ shows a slight intralayer contraction and a slight interlayer dilatation with respect to the structure of $Pb_2V_3O_9$. The way the XO_4 (X = V, As) tetrahedra twist and rotate depends on the intra- and interlayer spacing and should be responsible for different inter- and interlayer electrostatic interactions for $Pb_2V_3O_9$ and $Pb_2As_2VO_9$. Furthermore, in the 2D-planes, the difference between long and short V^{4+}-As^{5+} bonds (V1−As2 = 3.32 Å and 3.37 Å) is reduced. Other competing effects can predominate and stabilize the antiferro form. In fact, those effects certainly include the different role of As^{5+} compared with V^{5+} in terms of ionic radii, screening effects and orbital filling.

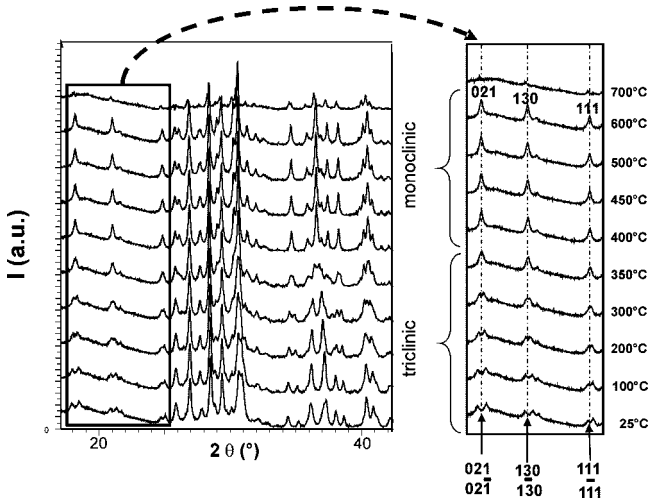

Figure 3. XRD pattern of $Pb_2V_3O_9$ under flowing nitrogen with evidence of the triclinic → monoclinic distortion.

Table 5. Atomic Coordinates and Isotropic/Equivalent Thermal Parameter at 550 °C (space group Cc)[a]

atom	*x*	*y*	*z*	U_{eq}
Pb1[i]	0.004(1)	0.12479(9)	0.2542(11)	0.0329(8)
Pb2	0	0.5467(1)	0.25	0.0411(9)
V1[ii]	−0.007(2)	0.3388(3)	0.247(2)	0.0026(9)
V3	−0.213(1)	0.2558(4)	0.5363(13)	0.007(1)
V2	−0.498(3)	0.4190(3)	0.255(3)	0.009 (1)
O1[iii]	−0.009(7)	0.716(1)	0.254(8)	0.006(5)
O2a	−0.348(7)	0.481(3)	0.218(9)	0.026(4)
O2b	0.335(7)	−0.475(3)	−0.221(8)	0.026(4)
O3a	−0.617(4)	0.354 (2)	0.018(5)	0.005(4)
O3b	0.660(4)	−0.364(2)	−0.013(5)	0.005(4)
O4a	−0.100(6)	0.403(2)	0.027(7)	0.020(4)
O4b	0.134(6)	−0.398(2)	−0.027(7)	0.020(4)
O5a	0.161(5)	0.274(2)	0.230(6)	0.014(4)
O5b	−0.170(5)	−0.281(2)	−0.214(6)	0.014(4)

[a] The Pb atoms were treated anisotropically but the vanadium atoms isotropically.

We were unable to prepare polycrystalline $Pb_2As_2VO_9$ samples free of minor amount of $Pb_3(AsO_4)_2$ impurity and unassigned minor XRD peaks. However, our Rietveld refinement shows that more than 95 wt % of the sample is $Pb_2As_2VO_9$. Strong preferred orientation effects were detected and were partially corrected to obtain the final $R_F = 5.36\%$, $R_{Bragg} = 6.61\%$, and $\chi^2 = 3.66\%$. This analysis supports the primitive lattice reminiscent of the particular vanadyl ordering in the polycrystalline sample. It is evidenced by weak *h*, *k*, *l*, $h + k = 2n+1$ lines in good agreement with the calculated XRD pattern (see Figure S2 of the Supporting Information).

Table 6. Atomic Coordinates for $Pb_2As_2VO_9$ and U_{eq} (Å^2)[a]

atom	*x*	*y*	*z*	U_{eq}
Pb1	0.0112(2)	0.12227(5)	0.2596(2)	0.0222(3)
Pb2	−0.0106(2)	0.53851(7)	0.2439(3)	0.0422(5)
As1	0.0057(4)	0.3359(1)	0.2539(5)	0.0136(7)
As2	−0.0026(4)	−0.0802(1)	0.2490(4)	0.0141(7)
V1	0.2196(7)	−0.2564(3)	0.4701(8)	0.020(2)
O1*	0.004(3)	−0.2823(8)	0.261(3)	0.014(3)
O2	−0.167(2)	0.278(1)	0.282(3)	0.018(6)
O3	0.135(2)	−0.142(1)	0.476(3)	0.017(3)
O4	0.165(2)	0.271(1)	0.230(3)	0.017(6)
O5	0.122(3)	0.399(1)	0.474(3)	0.018(6)
O6*	−0.132(3)	−0.140(1)	0.017(3)	0.019(6)
O7	−0.105(2)	0.397(1)	0.033(3)	0.019(7)
O8	−0.169(2)	−0.023(1)	0.283(3)	0.021(4)
O9	0.166(3)	−0.020(1)	0.237(4)	0.04(1)

[a] The thermal parameters for O1 and O6 were treated isotropically.

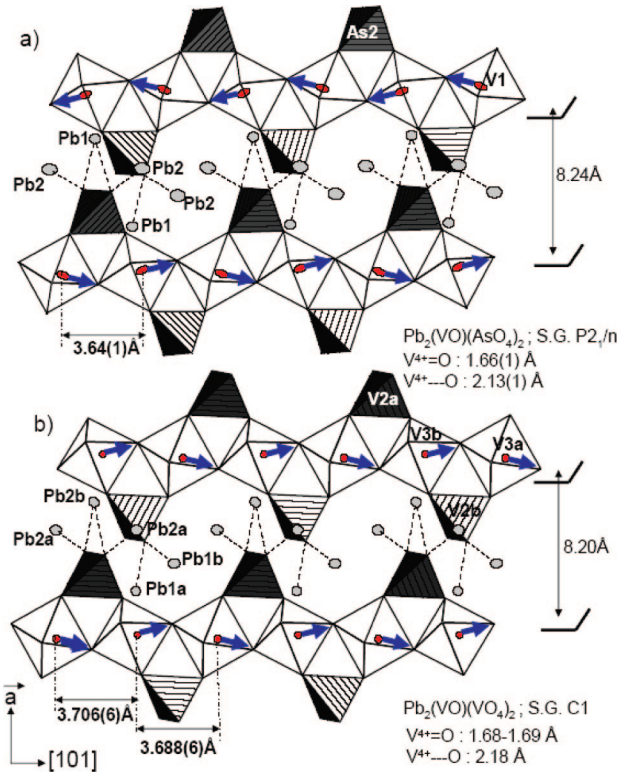

Figure 4. Comparison of the arrangements of the V^{4+}=O vanadyl bonds in the crystal structures of (a) $Pb_2As_2VO_9$ and (b) $Pb_2V_3O_9$.

4. Qualitative Evaluation of Spin Exchange Parameters

4.1. Spin Dimer Analysis. In spin dimer analysis based on extended Hückel tight-binding (EHTB) calculations,[14] the strength of a spin exchange interaction between two spin sites is estimated by considering only the AFM contribution J_{AF} to the spin exchange,

$$J_{AF} \approx -\frac{(\Delta\varepsilon)^2}{U_{eff}} \quad (1)$$

where U_{eff} is the effective on-site repulsion that is essentially a constant for a given compound. If the two spin sites are equivalent, $\Delta\varepsilon$ is the energy difference Δe between the two magnetic orbitals representing the spin dimer. When the two spin sites are nonequivalent, $(\Delta\varepsilon)^2 = (\Delta e)^2 - (\Delta e^0)^2$, where Δe^0 is the energy difference between the magnetic orbitals representing each spin site of the spin dimer ($\Delta e^0 = 0$ if the two spin sites are equivalent). In the present work, the $(\Delta\varepsilon)^2$ values for various spin dimers are evaluated by performing EHTB calculations.[21]

Table 7. Selected Interatomic Distances for $Pb_2As_2VO_9$ at $T = 298$ K

Pb^{2+} polyhedra				As^{5+} tetrahedra		V^{4+} octahedra	
Pb1−O2	2.94(2)	Pb2−O1	2.95(1)	As1−O2	1.70(2)	V1−O1	1.61(1)
−O3	2.60(2)	−O3	2.92(2)	−O4	1.69(2)	−O1	2.18(1)
−O4	2.76(2)	−O5	2.68(2)	−O5	1.69(1)	−O2	1.99(2)
−O5	2.62(1)	−O5	2.70(2)	−O7	1.67(2)	−O3	2.00(2)
−O6	2.53(2)	−O7	2.66(2)			−O4	2.03(2)
−O7	2.57(1)	−O7	2.70(2)	As2−O3	1.72(1)	−O6	1.98(2)
−O8	2.79(2)	−O8	2.55(2)	−O6	1.71(1)		
−O9	2.66(2)	−O9	2.72(3)	−O8	1.68(2)		
				−O9	1.65(3)		

For a variety of magnetic solids of transition metal ions, it has been found that their magnetic properties are well described by the $(\Delta\varepsilon)^2$ values obtained from EHTB calculations, when both the d orbitals of the transition metal ions and the s/p orbitals of its surrounding ligands are represented by double-ζ Slater-type orbitals.[22] The atomic parameters used in our calculations are summarized in Table S3 of the Supporting Information.

4.2. $Pb_2V_3O_9$. $Pb_2V_3O_9$ has two nonequivalent tetravalent V(3) atoms at octahedral sites, V(3a) and V(3b), as depicted in Figure 5a. If the long V(3)···O bond is neglected, each V(3a) or V(3b) atom forms a VO_5 square pyramid in which the distance between the V and the axial oxygen atom (V−O_{ax}, i.e., the vanadyl V=O bond) is considerably shorter than that between the V and the equatorial oxygen atoms (V−O_{eq}). In Figure 5a the V−O_{eq} bonds are indicated by shading. If the local *z*-axis of a VO_5 square pyramid is taken along the V−O_{ax} axis with the *x*- and *y*-axes approximately along the V−O_{eq} directions, then the d_{xy} level becomes the magnetic orbital of each VO_5 square pyramid, in which the d_{xy} orbitals of V^{4+} makes π-type antibonding interactions with the 2p orbitals of the O_{eq} atoms (Figure 5c). As shown in Figure 5b, there are four spin exchange paths J_1−J_4 to consider within each V_3O_9 layer. J_1 and J_2 are the nearest-neighbor V−O−V superexchange (SE) interactions in each chain of corner-sharing VO_6 octahedra, while J_3 and J_4 are the V−O···O−V super-superexchange (SSE) interactions between adjacent chains of corner-sharing VO_6 octahedra. The geometrical parameters associated with these spin exchange paths are summarized in Table 8.

Results of our spin dimer analysis are also summarized in Table 8, which reveals that the spin exchange interactions of $Pb_2V_3O_9$ are dominated by the SSE interactions J_3 and J_4, while the SE interactions J_1 and J_2 are negligible. The J_3 and J_4 interactions form alternating chains with the degree of alternation $\alpha = J_4/J_3$ of approximately 0.7. The latter is in reasonable agreement with the ratio $\alpha = 0.65$[2a] and 0.59[2b] deduced from the fitting analysis of the magnetic susceptibility of $Pb_2V_3O_9$. It should be noted that the alternating AFM chain model does not arise from the intrachain (namely, along

(21) (a) Hoffmann, R. *J. Chem. Phys.* **1963**, *39*, 1397. (b) Our calculations were carried out by employing the SAMOA (Structure and Molecular Orbital Analyzer) program package. http://chvamw.chem.ncsu.edu/ (This program can be downloaded free of charge from the website).

(22) Clementi, E.; Roetti, C. *Atomic Data Nuclear Data Tables* **1974**, *14*, 177.

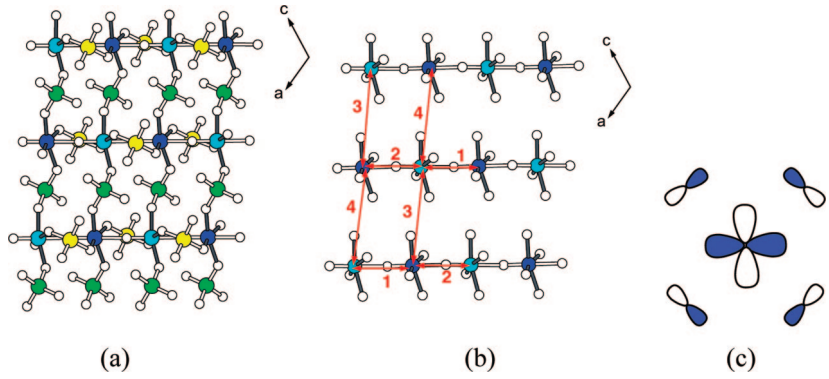

Figure 5. (a) Perspective view of an isolated V_3O_9 layer of $Pb_2V_3O_9$. The blue, cyan, yellow, green, and white circles represent the V(3a), V(3b), V(2), V(1), and O atoms, respectively. (b) Spin exchange paths of $Pb_2V_3O_9$. The numbers 1−4 represent the spin exchange paths J_1−J_4, respectively. (c) Magnetic orbital of a VO_5 square pyramid.

Table 8. Geometrical Parameters and $(\Delta\varepsilon)^2$ Values Associated with the SE and SSE Paths in $Pb_2V_3O_9$[a]

path	V···V (Å)	V−O (Å)	∠V−O−V (deg)	$(\Delta\varepsilon)^2$
		(a) SE		
J_1	3.688	1.682/2.188	144.4	41
J_2	3.706	1.695/2.187	145.0	130
		(b) SSE		
J_3	6.275	2.007/1.965	2.784	140.6/138.4 10700
J_4	6.319	2.036/1.981	2.784	130.5/153.8 7690

[a] The $(\Delta\varepsilon)^2$ values are in units of $(meV)^2$.

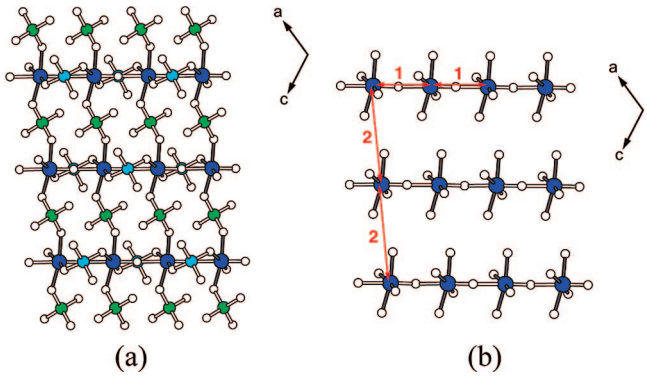

Figure 6. (a) Perspective view of an isolated As_2VO_9 layer of $Pb_2As_2VO_9$. The blues, green, cyan, and white circles represent the V, As(1), As(2), and O atoms, respectively. (b) Spin exchange paths of $Pb_2As_2VO_9$. The numbers 1 and 2 represent the spin exchange paths J_1 and J_2, respectively.

the V^{4+}═O···V^{4+}═O direction) but from the interchain spin exchange interactions. This finding is similar to that found for $Sr_2V_3O_9$, namely, the uniform AFM chain model describing this compound also arises from the interchain spin exchange interactions.[12]

4.3. $Pb_2As_2VO_9$. $Pb_2As_2VO_9$ has one kind of tetravalent V atoms at octahedral sites, As(1) and As(2) atoms at tetrahedral sites, as depicted in Figure 6a, where the V−O_{eq} bonds are indicated by shading. As shown in Figure 5b, there are two spin exchange paths J_1 and J_2 to consider within each As_2VO_9 layer. J_1 is the nearest-neighbor V−O−V SE interactions in each chain of corner-sharing VO_6 octahedra, while J_2 is the V−O···O−V SSE interaction between adjacent chains of corner-sharing VO_6 octahedra. The geometrical parameters associated with these spin exchange paths are summarized in Table 9. Results of our spin dimer

Table 9. Geometrical Parameters and $(\Delta\varepsilon)^2$ Values Associated with the SE and SSE Paths in $Pb_2As_2VO_9$[a]

path	V···V (Å)	V−O (Å)	∠V−O−V (deg)	$(\Delta\varepsilon)^2$
		(a) SE		
J_1	3.641	1.659/2.126	148.1	14
		(b) SSE		
J_2	6.295	2.000/2.014	2.721	146.7/135.4 13

[a] The $(\Delta\varepsilon)^2$ values are in units of $(meV)^2$.

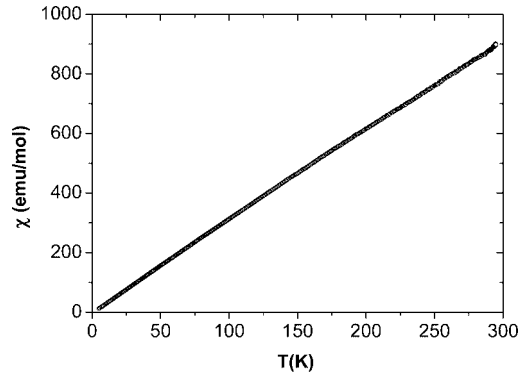

Figure 7. Plot of the inverse molar magnetic susceptibility of $Pb_2As_2VO_9$ as a function of temperature.

analysis, also summarized in Table 9, reveal that the spin exchange interactions J_1 and J_2 are both negligibly small. This predicts that the magnetic properties of $Pb_2As_2VO_9$ would be most likely paramagnetic. We confirmed this prediction by magnetic susceptibility measurements. The inverse molar magnetic susceptibility of $Pb_2As_2VO_9$ is plotted in Figure 7. (The susceptibility data were corrected for the sample holder and intrinsic paramagnetism. In addition, the presence of diamagnetic $Pb_3(As_2O_8)$ impurity (5%) was taken into consideration in obtaining the molar magnetic susceptibility.) It shows a nearly perfect Curie−Weiss behavior with $\mu_{eff} = 1.62\ \mu_B$ per formula unit and the very low Curie−Weiss temperature $\theta_{CW} = -2.2$ K. The effective moment is lower than expected from the spin-only approximation for one V^{4+} per formula unit (i.e., 1.73 μ_B), due possibly to the inaccuracy of the diamagnetic impurities. In any event, the paramagnetic behavior is in good agreement with the prediction.

(23) (a) Kresse, G.; Hafner, J. *Phys. Rev. B* **1993**, *62*, 558. (b) Kresse, G.; Furthmüller, J. *Comput. Mater. Sci.* **1996**, *6*, 15. (c) Kresse, G.; Furthmüller, J. *Phys. Rev. B* **1996**, *54*, 11169.

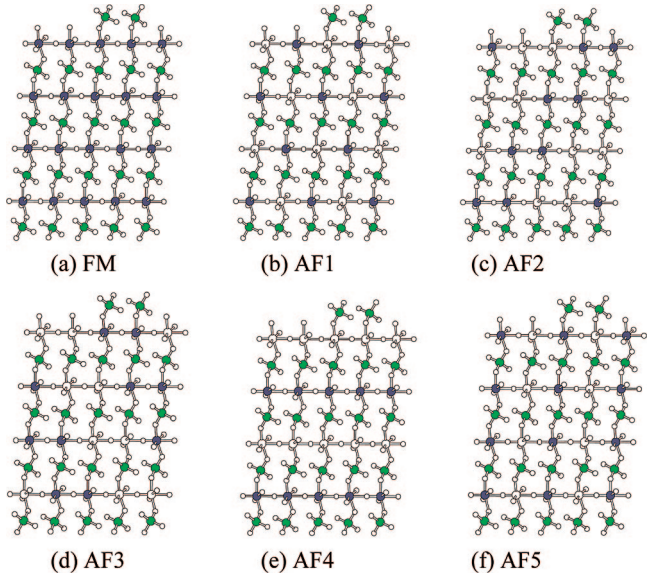

Figure 8. Ordered spin arrangements in the 2 × 1 × 2 supercell of $Pb_2V_3O_9$ where the gray and large white circles represent up-spin and down-spin V(3) sites, respectively. The green and small circles refer to bridging V atoms and oxygen atoms, respectively.

5. Quantitative Evaluation of Spin Exchange Interaction Parameters

In this section we determine the spin exchange parameters J_1-J_4 of $Pb_2V_3O_9$ on the basis of first principles DFT electronic band structure calculations. For this purpose, we first calculate the total energies of five ordered spin states of $Pb_2V_3O_9$ and then relate the energy differences between these states to the corresponding energy differences expected from the spin Hamiltonian,

$$\hat{H} = -\sum_{i<j} J_{ij}\hat{S}_i \cdot \hat{S}_j \qquad (2)$$

where J_{ij} (= J_1-J_4) is the spin exchange parameter for the spin exchange interaction between the spin sites i and j, while $\hat{S}_i$ and $\hat{S}_j$ are the spin angular momentum operators at the spin sites i and j, respectively. For our mapping analysis, we considered the six ordered spin arrangements using the 224-atom 2 × 1 × 2 supercell of $Pb_2V_3O_9$, as shown in Figure 8. The total energies of these states were calculated by performing spin-polarized DFT electronic band structure calculations with the projected augmented-wave method encoded in the Vienna ab initio simulation package.[23] Our calculations employed the generalized gradient approximation (GGA) for the exchange and correlation correction,[24] the plane wave cut off energy of 400 eV, the on-site repulsion U on copper, and the sampling of the Brillouin zone with the set of 2 × 2 × 2 k-points. To see how the value of U affects our results, we performed GGA plus onsite repulsion (GGA+U) calculations[25] with U = 3, 4, and 5 eV only on the V^{4+} sites.

Our GGA+U calculations show that the AF4 state is the most stable state. The relative energies of the eight ordered spin states with respect to that of the AF4 state are listed in Table 10. To extract the values of the spin exchange parameters J_1-J_4 from the above electronic structure calculations, we express the total spin exchange interaction energies of the six ordered spin states in terms of the spin Hamiltonian given in eq 2. By applying the energy expressions obtained for spin dimers with N unpaired spins per spin site (in the present case, N = 1),[26] the total spin exchange energies per formula units are written as

$$\begin{aligned}
E_{FM} &= (-8J_1 - 8J_2 - 8J_3 - 8J_4)(N^2/4)\\
E_{AF1} &= (8J_1 + 8J_2 + 8J_3 + 8J_4)(N^2/4)\\
E_{AF2} &= (-8J_1 + 8J_2 - 8J_3 + 8J_4)(N^2/4)\\
E_{AF3} &= (8J_1 - 8J_2 - 8J_3 + 8J_4)(N^2/4)\\
E_{AF4} &= (-8J_1 - 8J_2 + 8J_3 + 8J_4)(N^2/4)\\
E_{AF5} &= (8J_1 + 8J_2 - 8J_3 - 8J_4)(N^2/4)
\end{aligned} \qquad (3)$$

From the above equations, the spin exchange parameters J_1-J_4 can be expressed in terms of state energy differences as follows:

$$\begin{aligned}
J_1 &= (1/32)(4/N^2)\{(E_{AF1} - E_{AF4}) - (E_{AF2} - E_{AF3})\}\\
J_2 &= (1/16)\{(4/N^2)(E_{AF1} - E_{AF4}) - 16J_1\}\\
J_2 &= (1/16)\{(4/N^2)(E_{AF2} - E_{AF3}) + 16J_1\}\\
J_3 &= (1/16)\{(4/N^2)(E_{AF1} - E_{AF2}) - 16J_1\}\\
J_4 &= (1/16)\{(4/N^2)(E_{AF2} - E_{AF5}) + 16J_1\}
\end{aligned} \qquad (4)$$

The J_1-J_4 values calculated from the above expressions are summarized in Table 11.

For all values of U employed, the two strongest AFM spin exchange interactions are J_3 and J_4 with the ratio $J_4/J_3 \approx 0.7$, as found from the spin dimer analysis in the previous section. Note that J_1 and J_2 describe the intrachain interactions (from the viewpoint of corner-sharing VO_6 octahedra), while J_3 and J_4 describe the interchain interactions. Thus, the alternating AFM interactions occur between the ferromagnetic (FM) chains. Since J_1 and J_2 are substantially FM, it is of interest to examine how reasonable the calculated

Table 10. Relative Energies (meV) of the Ordered Spin States of $Pb_2V_3O_9$ Obtained from GGA+U Calculations

state	U = 3 eV	U = 4 eV	U = 5 eV
E_{FM}	15.1	9.7	6.3
E_{AF1}	14.4	14.1	14.2
E_{AF2}	15.7	12.5	10.7
E_{AF3}	17.0	13.5	11.5
E_{AF4}	0.0	0.0	0.0
E_{AF5}	30.2	24.3	20.9

Table 11. Values of the Spin Exchange Parameters (in k_BK) Determined from GGA+U Calculations

	U = 3 eV	U = 4 eV	U = 5 eV
J_1	23	22	22
J_2	19	19	19
J_3	−19	−17	−12
J_4	−27	−12	−8
J_4/J_3	0.70	0.71	0.67
θ_{cal} (K)	−1	3	5

(24) Perdew, J. P.; Burke, S.; Ernzerhof, M. *Phys. Rev. Lett.* **1996**, *77*, 3865.
(25) Dudarev, S. L.; Botton, G. A.; Savrasov, S. Y.; Humphreys, C. J.; Sutton, A. P. *Phys. Rev. B* **1998**, *57*, 1505.
(26) (a) Dai, D.; Whangbo, M.-H. *J. Chem. Phys.* **2001**, *114*, 2887. (b) Dai, D.; Whangbo, M.-H. *J. Chem. Phys.* **2003**, *118*, 29.

spin exchange parameters are by calculating the Curie−Weiss temperature θ in terms of these parameters. The θ value of $Pb_2V_3O_9$ is −12.3 K.[2] In the mean field theory,[27] which is valid in the paramagnetic limit, θ is related to the spin exchange parameters of $Pb_2V_3O_9$ as follows:

$$\theta_{cal} = \frac{S(S+1)}{3k_B}\sum_i z_i J_i = \frac{J_1 + J_2 + J_3 + J_4}{4k_B} \qquad (5)$$

where the summation runs over all nearest neighbors of a given spin site, z_i is the number of nearest neighbors connected by the spin exchange parameter J_i, and S is the spin quantum number of each spin site (i.e., $S = 1/2$ in the present case). The θ values estimated by using the calculated spin exchange parameters (i.e., θ_{cal}) are summarized in Table 11, which shows that the θ_{cal} is only slightly negative when $U = 3$ eV but positive for other values of U. This indicates that the FM interactions (J_1 and J_2) are overestimated compared with the AFM interactions (J_3 and J_4).

6. Concluding Remarks

An accurate structure of $Pb_2V_3O_9$ was determined by single crystal X-ray diffraction using a twinned crystal. An ambiguity remains about an ordering of the V^{4+}=O groups. However, XRD, structural, and electrostatic considerations suggest a probable ferro-like arrangement of vanadyl bonds in 2D-planes and between them. The resulting crystal structure adopts the *C*1 space group and differs substantially from its previous structure determined from a combined use of powder X-ray and neutron diffraction data. Both powder and single crystal diffraction data show a triclinic → monoclinic transition at around 450 °C. The latter is associated with the removal of the twinning inherent to the pseudomonoclinic symmetry of the low-temperature form. The crystal structure of the related arsenate $Pb_2As_2VO_9$ with interlayer Antiferro ordering of the vanadyl $bond_s$, also characterized in this work, is in support of the new crystal structure of PbV_3O_9.

The spin exchange interactions of PbV_3O_9, deduced by performing both qualitative spin dimer analysis and quantitative mapping analysis, shows that the magnetic properties of PbV_3O_9 should be described by an AFM alternating chain model, in agreement with experiment. The degree of alternation α of the alternating chain is calculated to be approximately 0.7, in reasonable agreement with experiment. The alternating spin−lattice chains are made up of the SSE interactions mediated by VO_4 tetrahedra between adjacent chains of corner-sharing VO_6 octahedra. Our spin dimer analysis of $Pb_2As_2VO_9$ predicts paramagnetic properties for $Pb_2As_2VO_9$, in agreement with experiment.

Acknowledgment. O.M. would like to thank Dr. V. Petricek for his modifications of Jana 2000 for twin processing and Dr. P. Roussel for discussion, as well as the "Fonds Européen de Développement Régional", "CNRS", "Région Nord Pas-de-Calais", and "Ministère de l'Education Nationale de l'Enseignement Supérieur et de la Recherche" for the funding of the X-ray diffractometers. The work at North Carolina State University was supported by the Office of Basic Energy Sciences, Division of Materials Sciences, U.S. Department of Energy, under Grant DE-FG02-86ER45259.

Supporting Information Available: The spin dimer analysis for $Pb_2V_3O_9$ using its old structure reported in ref 1, Tables S1−S3, and Figures S1 and S2 (PDF) as well as crystallographic information (CIF).This material is available free of charge via the Internet at http://pubs.acs.org.

CM800924J

(27) Smart, J. S. *Effective Field Theory of Magnetism*; Saunders: Philadelphia, 1966.